DOI:
10.1109/TMECH.2023.3287789

Document Version
Peer reviewed version

A Variable Impedance Scheme based on Power-Shaping Signals and Partial Knowledge of Link-Side Dynamics for Flexible-Joint Robot Interaction and Tracking Control

Emmanouil Spyrakos-Papastavridis[1], Jian S. Dai[1,2]

***Abstract*—This paper proposes a novel scheme – based on power-shaping control (PSC) – that can endow flexible-joint robots with both tracking, and interactional, capabilities. In virtue of relying upon the PSC method, this approach entails modest modelling requirements restricted to computation of the gravitational torque vector, and motor-side dynamics terms (typically available in manufacturer datasheets). Hence, it distinguishes itself by obviating the need for calculation of computationally cumbersome link-side dynamics elements, such as the Coriolis and link inertia matrices. In contrast to analogous schemes, the highest-order term required by the proposed design is the third derivative of the motor position vector; it therefore avoids the usage of link-jerk feedback that can be detrimental to interactional performance. Moreover, the propounded framework enables utilisation of non-collocated feedback for enhanced tracking accuracy, as well as variable impedance control (VIC) for interactional performance augmentation. The aforesaid features are effectuated without any reliance on coordinate transformations; thus, the original dynamical model's structure remains immutable throughout. Also, the proposed design's complexity is dependent solely on the gravitational torque vector's dimension (i.e. not on the link inertia or Coriolis terms). Experimental results involving a flexible-joint robot, namely the Rethink Robotics Baxter, corroborate the theoretical analyses, in addition to demonstrating that interactional performance improvements can be achieved via the proposed methodology.**

I. Introduction

Due to the ever-increasing demand for safe coexistence of humans and robots, within human-inhabited environments, the topic of physical human-robot interaction (pHRI) has gained considerable popularity. pHRI methodologies are typically divided into two main categories, namely those that pertain to hardware design, and those relating to software development. In terms of the latter category, indirect force control techniques – including several permutations of impedance control methods which are described in detail in [1] – seem to prevail among roboticists, as compared to direct force controllers. This may in part be attributed to the implementational complexity of direct force controllers, which typically rely on environmental modelling, and/or direct usage of force feedback. Contrariwise, impedance control (originally introduced in [2]), qua indirect force control, relies on a contact-model-free approach, which, however, also offers the user a degree of tractability over the dynamical interactions between the robot and its environment [3]. Examining the existing literature on this subject allows one to conclude that there is an array of works pertaining to impedance control—earlier treatises introduced its theoretical foundations [2][3], while subsequent research efforts have been directed towards experimental corroboration [4][5].

It is posited that interactional performance can be further improved through online modulation of a robot's active impedance gains – a methodology that is typically referred to as variable impedance control (VIC) [6][7]. As a matter of fact, some works [8] even postulate that the superior interactional, and locomotion, performance exhibited by biological machines is a direct result of the level of sophistication of their immanent VIC mechanisms (i.e. muscular activity).

In contrast to software-related techniques, robotic hardware design research attempts to effectuate interactional performance enhancement through direct incorporation of passive elastic elements into a robot's mechanical composition [9][10]. This design category can be further divided into two subcategories: flexible-joint [9] and flexible-link [10] robots. There is a contemporary tendency to refer to these former devices as articulated soft robots (ASRs) [11]. The category of ASRs comprises those that are powered by Series Elastic Actuators (SEAs) [9][12], as well as those containing harmonic drives [13]. In spite of their improved interactional robustness, owing to the force attenuation capability of their physical springs, SEA-powered robots are unable to alter their passive stiffnesses in a real-time fashion; a shortcoming that may be bypassed through employment of Variable Stiffness Actuators (VSAs) [14][15]. Even though VSAs can enhance interactional robustness and performance, their design and usage typically imply increased dimensional requirements, control complexity, and design cost.

As a result, numerous works [11][15] revolve around the unification of physical, and software-induced, flexibility, via practical implementation of impedance controllers on ASRs, to augment their interactional performance.

Set-point regulation control of ASRs is a deeply investigated research topic, boasting several well-established methodologies [16][17]. In spite of these works, strong stability results are more difficult to acquire when dealing with the challenging problem of trajectory-tracking control of ASRs [13][18][19][20][21]. Existing treatises on the latter subject propound heavily model-based solutions necessitating high-order derivatives of dynamics matrices, as well as of position variables. To this end, a more recent work proposes a near-model-free technique (as it still requires a spring stiffness model) for the control of compliant joint robots with linear stiffness joints [22], while another propounds a model-based controller relying upon simplified dynamical models

[1]Department of Engineering, King's College London, Strand, London, WC2R 2LS, United Kingdom. [2]Southern University of Science and Technology, Shenzhen 518055, Guangdong, China.

that intentionally neglect the motor dynamics [23]. However, modelling only the motor dynamics can be deemed preferable, since rotor inertia and (sometimes) damping parameters are typically contained within motor manufacturer datasheets (or provided upon request); also, the motor dynamics models of ASRs are often deemed linear, e.g. [11][15][18][24][33]. An additional complication arises from the fact that most of the existing, ASR tracking controllers are exclusively applicable to linear stiffness robots [18]. However, [18][20][24] propose schemes for nonlinear stiffness robots, while [19][20][25] also consider time-varying, active impedance parameters (VIC). Some works [26]-[29] even report on the usage of VIC methods on flexible-joint, bipedal robots. Despite VIC's ability to yield improved tracking and interactional performance [30], one must exercise caution when increasing a system's active stiffness gain values (in real-time), as these can be detrimental to closed-loop stability/passivity [31]. To this end, [31] introduces a tank-based controller to ensure passivity, via suppression of the energy injections induced during the stiffness-increasing phases. [30] demonstrates that through the creation of a novel Lyapunov function, it is possible to derive gain modulation rate conditions whose satisfaction guarantees closed-loop stability; [32] enhances this framework by considering variable damping gains. Further, [33] extends the applicability of tank-based schemes to redundant robots. However, the forenamed methods are tailored to rigid-joint robots, and this precludes direct transferability to ASRs. To bridge this gap, [19][20][25]-[27] propose various schemes – based on the Power-Shaping Control (PSC) design concept – that can guarantee stability/passivity for VIC of: ASRs [19][20]; floating-base robots with contacts [34]; floating-base ASRs with contacts [26][27].

The PSC design idea exploited herein employs a direct solution to underactuation, influenced by the approaches described in [19][20][25]-[27], thereby addressing the issues that have been outlined throughout this section. Thus, the controllers proposed in this work inherit all the features of the schemes delineated in [19][20][25]-[27], namely:

- Stability-guaranteed, unrestrained gain modulation during VIC.
- Applicability to nonlinear stiffness robots.
- Usage of collocated and non-collocated state feedback.

The remainder of this article commences with Section II, which synopsises a number of related works to highlight the proposed method's contributions; Section III introduces the nonlinear impedance, flexible-joint robot model, while Section IV provides an overview of the control design aims and proposed controller architecture; Section V describes the extensions required to ensure stable VIC, applicability to nonlinear-stiffness-joint robots, and saturation prevention (energy efficiency); Section VI presents the experimental results; Section VII offers the conclusion.

II. Related Works

One of the main difficulties with the existing ASR tracking controllers (those that offer stability guarantees) is that they typically rely upon heavily model-based solutions. This fact renders them relatively complex in terms of implementation, as they require computation of the link inertia and Coriolis terms, which may be more difficult to derive than the gravitational torque vector, and certainly more so than the motor dynamics. Lagrangian dynamics (symbolic) formulations are intractable for systems comprising $n \geq 7$ joints, and this then necessitates usage of recursive algorithms [35], whose inertia matrix calculations are of $O(n^2)$ algorithmic complexity. Contrarily, gravitational torque vector calculations are of markedly lower complexity. Most importantly, the presence of higher-order position derivatives, and, in particular, the link acceleration and jerk variables, can have a detrimental effect on interactional performance [21][36]. To mitigate the effect of these *link* jerk signals contained in the controllers, [21] proposes the use of "dirty" derivatives, while [36] introduces a damping design method based on dynamic extensions. As compared to the methods presented in [19][20][25]-[27], and to other, existing ASR trajectory-tracking control designs, the controllers proposed in this work make the following contributions:

- Stability-guaranteed (global asymptotical) tracking control of ASRs is achieved, for the first time, in the absence of the link inertia and Coriolis matrices, i.e. using uncomplicated model-based signals (lower modelling requirements); thus, these PSC controllers are considerably simpler to implement compared to other relevant designs in the literature that offer stability guarantees [13][18][19][20][21][25]. Also, [13] is not specifically designed for interactional tasks, it relies on a complex control law (as stated in [13]), and has only been verified via simulation. On the other hand, [21] induces semiglobal asymptotical stability.
- Significantly improved interactional performance, due to the absence of link inertia and Coriolis terms (and therefore of their derivatives) from the controller, as well as of higher-order, link position derivatives (acceleration, jerk) [21][36]. These terms are predisposed to saturating the controller when the robot is subjected to impacts.
- In contrast to the aforementioned works, the proposed PSC schemes enable the robot to modulate its gains (while offering stability guarantees) through VIC, thereby possessing the ability to further improve interactional performance, as described in [6][8].

III. Visco-Elastic-Joint Robot Modelling

A. Visco-Elastic-Joint Robot Model

Robotic systems that are powered by actuators of non-negligible elasticity are typically termed flexible-joint robots, or ASRs. Following [37]'s paradigm, one may model an n-joint robot comprising linear stiffness and damping joints, powered by n actuators, in the following manner:

$$\mathbf{M}(\boldsymbol{q})\ddot{\boldsymbol{q}} + \mathbf{C}\dot{\boldsymbol{q}} + \mathbf{D}\left(\dot{\boldsymbol{q}} - \dot{\boldsymbol{\theta}}\right) + \mathbf{K}(\boldsymbol{q} - \boldsymbol{\theta}) + \boldsymbol{\tau}_{\boldsymbol{g}}(\boldsymbol{q}) = \boldsymbol{\tau}_{\boldsymbol{e}}, \quad (1)$$

$$\mathbf{J}\ddot{\boldsymbol{\theta}} + \mathbf{D}\left(\dot{\boldsymbol{\theta}} - \dot{\boldsymbol{q}}\right) + \mathbf{K}(\boldsymbol{\theta} - \boldsymbol{q}) = \boldsymbol{\tau}_{\boldsymbol{m}}, \quad (2)$$

where $\boldsymbol{q} \in \mathbb{R}^n$ and $\boldsymbol{\theta} \in \mathbb{R}^n$ denote the link and motor positions, while $\mathbf{M}(\boldsymbol{q})$, $\mathbf{C} \in \mathbb{R}^{n \times n}$ signify the symmetric inertia, and skew-symmetric Coriolis, matrices, respectively.

Moreover, $\boldsymbol{\tau_g(q)} \in \mathbb{R}^n$, $\boldsymbol{\tau_e} \in \mathbb{R}^n$, and $\boldsymbol{\tau_m} \in \mathbb{R}^n$ represent the gravitational, external, and input torque vectors, respectively. Finally, $\mathbf{K}$, $\mathbf{J}$, and $\mathbf{D} \in \mathbb{R}^{n\times n}$ denote the diagonal, positive definite stiffness, motor inertia, and joint damping matrices. If $\mathbf{C}$ is represented via Christoffel symbols, then the $\boldsymbol{\dot{q}^T}\big(\dot{\mathbf{M}} - 2\mathbf{C}\big)\boldsymbol{\dot{q}} = \mathbf{0}$ property holds true, as described in [38].

B. Non-Linear Visco-Elastic Elements

By following [37]'s approach, an n-DoF, nonlinear visco-elastic-joint robot can be modelled as follows:

$$\mathbf{M}\ddot{\boldsymbol{q}} + \mathbf{C}\dot{\boldsymbol{q}} + \mathbf{D}(t)\big(\dot{\boldsymbol{q}} - \dot{\boldsymbol{\theta}}\big) + \mathbf{K}(t)(\boldsymbol{q} - \boldsymbol{\theta}) + \boldsymbol{\tau_{gq}} = \boldsymbol{\tau_e}, \quad (3)$$

$$\mathbf{J}\ddot{\boldsymbol{\theta}} + \mathbf{D}(t)\big(\dot{\boldsymbol{\theta}} - \dot{\boldsymbol{q}}\big) + \mathbf{K}(t)(\boldsymbol{\theta} - \boldsymbol{q}) = \boldsymbol{\tau_m}, \quad (4)$$

where $\boldsymbol{\tau_{gq}} = \boldsymbol{\tau_g(q)}$, and $\mathbf{K}(t)$, $\mathbf{D}(t) \in \mathbb{R}^{n\times n}$ denote diagonal, positive definite, time-varying stiffness and viscous damping matrices, i.e. nonlinear stiffness/damping phenomena.

IV. An Uncomplicated Model-Based Scheme

A. PSC Method Mechanics: A General Summary

The schemes proposed in this work rely upon utilisation of the PSC design method [19][20][25][26][27][34], for the purpose of attaining global asymptotical stability. At its core, PSC functions by means of directly cancelling out any terms present in the Lyapunov function's derivative (a power function) – which may otherwise be ineliminable using conventional methods – thereby ensuring stability. To this end, a power-shaping torque is included within the overall control law used on the robot, which is typically of the form:

$$\boldsymbol{\tau}_{PSS_G} = \dot{\mathbf{Q}}_{\mathrm{G}}\boldsymbol{I}_{RG}p_{ss},$$

where $\dot{\mathbf{Q}}_{\mathrm{G}} = diag(\dot{\boldsymbol{q}}_G)^+ \in \mathbb{R}^{k\times k}$, the rank-normalised, all-ones vector, $\boldsymbol{I}_{RG} = [1 \dots 1_k]^T \cdot rank\big(\dot{\mathbf{Q}}_{\mathrm{G}}\big)^+ \in \mathbb{R}^k$, with $\boldsymbol{q}_G \in \mathbb{R}^k$ denoting a vector of generalised coordinates typically – but not necessarily – pertaining to the underactuated states. The user may then design p_{ss} in such a way as to ensure that all the undesirable terms are eliminated from the Lyapunov function's derivative. Thus, p_{ss} contains a number of scalar, "power" terms, whose signs are inverted w.r.t those present in the Lyapunov function's derivative (to cancel them out).

B. PSC via First-Order Link-Side Dynamics: Requirements

Although regulation control of ASRs is a well-established topic [16][17], tracking control constitutes a significantly more complex task [13][18]-[20][21][24]. Asymptotically stabilising designs typically necessitate an array of model-based terms, in addition to time derivatives of dynamics matrices and generalised coordinates (up to the fifth order). Therefore, at this initial stage, the aim is to produce a design capable of yielding a globally asymptotically stable (GAS), closed-loop tracking system, using terms of the lowest order possible, while excluding link jerk feedback, which can be detrimental to interactional control performance [21][36]. Moreover, to endow the scheme with interactional capabilities, impedance control terms are also required. Hence, the following PSC-based scheme is proposed:

$$\boldsymbol{\tau_m} = \mathbf{K}_{\mathbf{P_M}}\boldsymbol{\theta_E} + \mathbf{K}_{\mathbf{D_M}}\dot{\boldsymbol{\theta}}_{\boldsymbol{E}} + \mathbf{K}_{\mathbf{P_J}}\boldsymbol{q}_{\boldsymbol{E_S}} + a_{v1}\mathbf{K}_{\mathbf{D_J}}\dot{\boldsymbol{q}}_{\boldsymbol{E}} + \boldsymbol{\tau_{MD}} + a_{v0}\boldsymbol{\tau_{C0}} + \boldsymbol{\tau_{PSS}}, \quad (5)$$

where $\mathbf{K}_{\mathbf{P_M}}$, $\mathbf{K}_{\mathbf{D_M}}$, $\mathbf{K}_{\mathbf{P_J}}$, and $\mathbf{K}_{\mathbf{D_J}} \in \mathbb{R}^{n\times n}$ denote diagonal, positive definite, motor and link, active stiffness and damping matrices. Moreover, the motor and link position error vectors are denoted as $\boldsymbol{\theta_E} = \boldsymbol{\theta_d} - \boldsymbol{\theta}$, $\boldsymbol{q_E} = \boldsymbol{q_d} - \boldsymbol{q}$, and $\boldsymbol{q_{E_S}} = a_{vs}\boldsymbol{q_d} - \boldsymbol{q}$; a_{v0} and a_{v1} are scalar terms activated (i.e. equal to 1) when $\dot{\boldsymbol{\theta}}_{\boldsymbol{E}} = \mathbf{0}$, and $\dot{\boldsymbol{\theta}}_{\boldsymbol{E}} \neq \mathbf{0}$, respectively, and are otherwise deactivated (Appendix B). In an analogous manner, a_{vs} is nullified only when $\dot{\boldsymbol{\theta}}_{\boldsymbol{E}} = \mathbf{0}$, $\dot{\boldsymbol{q}} \neq \mathbf{0}$, and is defined as:

$$a_{vs} = (1 - a_{a1} + a_{v1})(1 - a_{a1} + a_{v1})^+, \quad (6)$$

where a_{a1} signifies a scalar that is set to 1 when $\dot{\boldsymbol{q}} \neq \mathbf{0}$, and to 0 otherwise. $\boldsymbol{\tau_{PSS}}$ symbolises the power-shaping torque that cancels out the otherwise-ineliminable terms appearing in the Lyapunov derivative function, while $\boldsymbol{\tau_{C0}}$ signifies a torque input used to eliminate any residual elements existing when $\dot{\boldsymbol{\theta}}_{\boldsymbol{E}} = \mathbf{0}$, and can be constructed through the equation:

$$\boldsymbol{\tau_{C0}} = \mathbf{K}(\boldsymbol{\theta_e} - \boldsymbol{q_e}) + \mathbf{J}\ddot{\boldsymbol{\theta}}_{\boldsymbol{e}} - \mathbf{D}\dot{\boldsymbol{q}}_{\boldsymbol{e}}, \quad (7)$$

where $\boldsymbol{\theta_e} = \boldsymbol{\theta} - \boldsymbol{\theta_d}$ and $\boldsymbol{q_e} = \boldsymbol{q} - \boldsymbol{q_d}$. The motor-dynamics-based torque, $\boldsymbol{\tau_{MD}}$, whose expression is provided below:

$$\boldsymbol{\tau_{MD}} = \mathbf{J}\ddot{\boldsymbol{\theta}}_{\boldsymbol{d}} + \mathbf{D}\big(\dot{\boldsymbol{\theta}}_{\boldsymbol{d}} - \dot{\boldsymbol{q}}_{\boldsymbol{d}}\big) + \mathbf{K}(\boldsymbol{\theta_d} - \boldsymbol{q_d}), \quad (8)$$

is employed to obtain motor-error dynamics. It now needs to be highlighted that to preserve the scheme's reduced reliance upon link-side dynamics terms, one must ensure that link-to-motor position conversions can be achieved through a simple relationship, such as the following:

$$\boldsymbol{\tau_{gd}} = \mathbf{K}(\boldsymbol{\theta_d} - \boldsymbol{q_d}), \quad (9)$$

where $\boldsymbol{\tau_{gd}} = \boldsymbol{\tau_g(q_d)}$. One means of enabling usage of such an equation for higher order conversions is by "forcing" $\dot{\boldsymbol{q}}$ to $\mathbf{0}$, when $\dot{\boldsymbol{\theta}}_{\boldsymbol{E}} = \mathbf{0}$. As will be subsequently revealed, ensuring that $\dot{\boldsymbol{q}} = \mathbf{0}$ when $\dot{\boldsymbol{\theta}}_{\boldsymbol{E}} = \mathbf{0}$ guarantees that no uncompensated terms remain in the Lyapunov function's derivative; this is not achieved in either [20] or [26], which, unlike this work, require computation of the link inertia and Coriolis matrices.

Lemma 1: Setting $\dot{\boldsymbol{\theta}}_{\boldsymbol{E}} = \mathbf{0}$ and $\dot{\boldsymbol{q}} \neq \mathbf{0}$ in the closed-loop system comprising equations (3)-(5), yields:

$$\mathbf{K}_{\mathbf{P_M}}\boldsymbol{\theta_E} = \mathbf{K}_{\mathbf{P_J}}\boldsymbol{q}, \quad (10)$$

with $\mathbf{K}_{\mathbf{P_J}}$ denoting an invertible, symmetric, positive definite matrix, which therefore conduces to:

$$\boldsymbol{q} = \mathbf{K}_{\mathbf{P_J}}^{-\mathbf{1}}\mathbf{K}_{\mathbf{P_M}}\boldsymbol{\theta_E}. \quad (11)$$

Inasmuch as $\boldsymbol{\theta_E} = const.$, owing to $\dot{\boldsymbol{\theta}}_{\boldsymbol{E}} = \mathbf{0}$, it can then be concluded that $\boldsymbol{q} = const.$, and that $\dot{\boldsymbol{q}} = \mathbf{0}$, provided that $\mathbf{K}_{\mathbf{P_M}}$

and $\mathbf{K_{P_J}}$ are kept constant at that *instant*. However, if the system is already at the $\dot{\boldsymbol{\theta}}_{\boldsymbol{E}} = \mathbf{0}$, $\dot{\boldsymbol{q}} = \mathbf{0}$ state, then:

$$\boldsymbol{q}_{\boldsymbol{E}} = -\mathbf{K}_{\mathbf{P_J}}^{-1}\mathbf{K}_{\mathbf{P_M}}\boldsymbol{\theta}_{\boldsymbol{E}} = constant, \quad (12)$$

and $\dot{\boldsymbol{q}}_{\boldsymbol{E}} = \mathbf{0}$. This implies elimination of all undesirable, Lyapunov derivative terms, as will be subsequently revealed.

C. PSC plus Partial Link-Side Dynamics: Stability Analysis

Theorem 1: The closed-loop system comprising equations (3)-(5) possesses a GAS equilibrium point at $\boldsymbol{q}_{\boldsymbol{eq}} = \begin{bmatrix}\dot{\boldsymbol{q}}^T & \dot{\boldsymbol{\theta}}_{\boldsymbol{E}}^T & \boldsymbol{q}_{\boldsymbol{E_S}}^T & \boldsymbol{\theta}_{\boldsymbol{E}}^T\end{bmatrix} = \mathbf{0}$, when $\boldsymbol{\tau}_{\boldsymbol{e}} = \mathbf{0}$, provided that $\dot{\mathbf{K}}_{\mathbf{P_M}} = \dot{\mathbf{K}}_{\mathbf{P_J}} = \mathbf{0}$ when $\dot{\boldsymbol{\theta}}_{\boldsymbol{E}} = \mathbf{0}$.

Proof 1: The closed-loop system stability analysis revolves around the following Lyapunov function:

$$V = \tfrac{1}{2}\dot{\boldsymbol{q}}_{\boldsymbol{F_T}}^T\mathbf{M_T}\dot{\boldsymbol{q}}_{\boldsymbol{F_T}} + \tfrac{1}{2}\boldsymbol{\theta}_{\boldsymbol{E}}^T\mathbf{K}_{\mathbf{P_M}}\boldsymbol{\theta}_{\boldsymbol{E}} + \tfrac{1}{2}\boldsymbol{q}_{\boldsymbol{E_S}}^T\mathbf{K}_{\mathbf{P_J}}\boldsymbol{q}_{\boldsymbol{E_S}}, \quad (13)$$

where $\mathbf{M_T} = diag(\mathbf{M}, \mathbf{J})$, and $\boldsymbol{q}_{\boldsymbol{F_T}} = [\boldsymbol{q}^T \quad \boldsymbol{\theta}_{\boldsymbol{e}}^T]^T$. The above function is nullified solely at the origin, $\boldsymbol{q}_{\boldsymbol{eq}} = \mathbf{0}$ (Appendix A), and is positive elsewhere, while its time derivative is[1]:

$$\dot{V} = \dot{\boldsymbol{q}}_{\boldsymbol{F_T}}^T\left(\begin{array}{c}\frac{\dot{\mathbf{M}}_{\mathbf{T}}\dot{\boldsymbol{q}}_{\boldsymbol{F_T}}}{2} - \mathbf{C_T}\dot{\boldsymbol{q}}_{\boldsymbol{F_T}} - \begin{bmatrix}\boldsymbol{\tau}_{\boldsymbol{gq}} - \mathbf{D}\dot{\boldsymbol{\theta}} - \mathbf{K}\boldsymbol{\theta} \\ -\mathbf{D}\dot{\boldsymbol{q}}_{\boldsymbol{e}} - \mathbf{K}\boldsymbol{q}_{\boldsymbol{e}}\end{bmatrix} - \boldsymbol{\Psi}\dot{\boldsymbol{q}}_{\boldsymbol{F_T}} - \\ \mathbf{K_T}\boldsymbol{q}_{\boldsymbol{F_T}} + \begin{bmatrix}\mathbf{0} \\ \mathbf{K}_{\mathbf{P_M}}\boldsymbol{\theta}_{\boldsymbol{E}} + \mathbf{K}_{\mathbf{P_J}}\boldsymbol{q}_{\boldsymbol{E_S}} + \mathbf{K}_{\mathbf{D_J}}\dot{\boldsymbol{q}}_{\boldsymbol{E}} + \boldsymbol{\tau}_{\boldsymbol{PSS}}\end{bmatrix}\end{array}\right) + \dot{\boldsymbol{\theta}}_{\boldsymbol{E}}^T\mathbf{K}_{\mathbf{P_M}}\boldsymbol{\theta}_{\boldsymbol{E}} + \dot{\boldsymbol{q}}_{\boldsymbol{E_S}}^T\mathbf{K}_{\mathbf{P_J}}\boldsymbol{q}_{\boldsymbol{E_S}}, \quad (14)$$

where $\boldsymbol{\Psi} = diag(\mathbf{D}, \mathbf{D} + \mathbf{K}_{\mathbf{D_M}})$, $\mathbf{C_T} = diag(\mathbf{C}, \mathbf{0})$, and $\mathbf{K_T} = diag(\mathbf{K}, \mathbf{K})$. Further simplifications – relying on the $\dot{\boldsymbol{q}}^T(\dot{\mathbf{M}} - 2\mathbf{C})\dot{\boldsymbol{q}} = \mathbf{0}$ property – produce:

$$\begin{aligned}\dot{V} = &-\dot{\boldsymbol{q}}^T\boldsymbol{\tau}_{\boldsymbol{gq}} + \dot{\boldsymbol{q}}^T\mathbf{D}\dot{\boldsymbol{\theta}} + \dot{\boldsymbol{q}}^T\mathbf{K}\boldsymbol{\theta} + \dot{\boldsymbol{\theta}}_{\boldsymbol{e}}^T\mathbf{K}\boldsymbol{q}_{\boldsymbol{e}} + \dot{\boldsymbol{\theta}}_{\boldsymbol{e}}^T\mathbf{D}\dot{\boldsymbol{q}}_{\boldsymbol{e}} - \\ &\dot{\boldsymbol{q}}_{\boldsymbol{F_T}}^T\boldsymbol{\Psi}\dot{\boldsymbol{q}}_{\boldsymbol{F_T}} - \dot{\boldsymbol{q}}_{\boldsymbol{F_T}}^T\mathbf{K_T}\boldsymbol{q}_{\boldsymbol{F_T}} + \dot{\boldsymbol{\theta}}_{\boldsymbol{e}}^T\mathbf{K}_{\mathbf{P_M}}\boldsymbol{\theta}_{\boldsymbol{E}} + \dot{\boldsymbol{\theta}}_{\boldsymbol{e}}^T\mathbf{K}_{\mathbf{P_J}}\boldsymbol{q}_{\boldsymbol{E_S}} + \\ &\dot{\boldsymbol{\theta}}_{\boldsymbol{e}}^T\mathbf{K}_{\mathbf{D_J}}\dot{\boldsymbol{q}}_{\boldsymbol{E}} + \dot{\boldsymbol{\theta}}_{\boldsymbol{e}}^T\boldsymbol{\tau}_{\boldsymbol{PSS}} + \dot{\boldsymbol{\theta}}_{\boldsymbol{E}}^T\mathbf{K}_{\mathbf{P_M}}\boldsymbol{\theta}_{\boldsymbol{E}} + \dot{\boldsymbol{q}}_{\boldsymbol{E_S}}^T\mathbf{K}_{\mathbf{P_J}}\boldsymbol{q}_{\boldsymbol{E_S}}. \quad (15)\end{aligned}$$

According to *Lemma 1*, all the $\dot{V}$ terms vanish when $\dot{\boldsymbol{\theta}}_{\boldsymbol{E}} = \dot{\boldsymbol{q}} = \mathbf{0}$. Although some of the above terms cancel out with one another, others ought to be expunged independently. Hence, the power-shaping torque is of the following form:

$$\boldsymbol{\tau}_{\boldsymbol{PSS}} = \dot{\boldsymbol{\Theta}}_{\mathbf{P}}\boldsymbol{I}_{\boldsymbol{R}}p_{ss}, \quad (16)$$

where $\dot{\boldsymbol{\Theta}}_{\mathbf{P}} = diag(\dot{\boldsymbol{\theta}}_{\boldsymbol{e}})^+ \in \mathbb{R}^{n\times n}$, and the rank-normalised, all-ones vector, $\boldsymbol{I}_{\boldsymbol{R}} = [1 \ldots 1_n]^T \cdot rank(\dot{\boldsymbol{\Theta}}_{\mathbf{P}})^+ \in \mathbb{R}^n$. Also, the PSS is designed in the following manner:

$$\begin{aligned}p_{ss} = &\dot{\boldsymbol{q}}^T\boldsymbol{\tau}_{\boldsymbol{gq}} + \dot{\boldsymbol{q}}_{\boldsymbol{F_T}}^T\mathbf{K_T}\boldsymbol{q}_{\boldsymbol{F_T}} - \dot{\boldsymbol{\theta}}_{\boldsymbol{e}}^T\mathbf{K}_{\mathbf{P_J}}\boldsymbol{q}_{\boldsymbol{E_S}} - \dot{\boldsymbol{q}}_{\boldsymbol{E_S}}^T\mathbf{K}_{\mathbf{P_J}}\boldsymbol{q}_{\boldsymbol{E_S}} - \\ &\dot{\boldsymbol{\theta}}_{\boldsymbol{e}}^T\mathbf{K}_{\mathbf{D_J}}\dot{\boldsymbol{q}}_{\boldsymbol{E}} - \dot{\boldsymbol{q}}^T(\mathbf{D}\dot{\boldsymbol{\theta}} + \mathbf{K}\boldsymbol{\theta}) - \dot{\boldsymbol{\theta}}_{\boldsymbol{e}}^T(\mathbf{D}\dot{\boldsymbol{q}}_{\boldsymbol{e}} + \mathbf{K}\boldsymbol{q}_{\boldsymbol{e}}). \quad (17)\end{aligned}$$

[1]The upper row of the expression between brackets is based on the original link dynamics (equation (1) or (3)), hence why it is possible to avoid utilisation of link inertia and Coriolis/centrifugal elements in the control law.

In virtue of the introduced elements, the following simplification takes place in the $\dot{V}$ function:

$$\dot{\boldsymbol{\theta}}_{\boldsymbol{e}}^T \cdot diag(\dot{\boldsymbol{\theta}}_{\boldsymbol{e}})^+ \cdot [1 \ldots 1_n]^T \cdot rank(\dot{\boldsymbol{\Theta}}_{\mathbf{P}})^+ = {}^n/_n = 1, \quad (18)$$

and then using the proposed p_{ss} results in:

$$\dot{V} = -\dot{\boldsymbol{q}}_{\boldsymbol{F_T}}^T\boldsymbol{\Psi}\dot{\boldsymbol{q}}_{\boldsymbol{F_T}}. \quad (19)$$

The analysis performed thus far has only treated the case where $\dot{\boldsymbol{\Theta}}_{\mathbf{P}}$ has full rank. If $\dot{\boldsymbol{\Theta}}_{\mathbf{P}}$ loses rank, then one obtains:

$$\dot{V} = -\dot{\boldsymbol{q}}_{\boldsymbol{F_T}}^T\boldsymbol{\Psi}\dot{\boldsymbol{q}}_{\boldsymbol{F_T}} + s_v + \tfrac{n-1}{n-1}\cdot p_{ss}, \quad (20)$$

where s_v contains all the terms in (15) excluding $\dot{\boldsymbol{q}}_{\boldsymbol{F_T}}^T\boldsymbol{\Psi}\dot{\boldsymbol{q}}_{\boldsymbol{F_T}}$ and $\dot{\boldsymbol{\theta}}_{\boldsymbol{e}}^T\boldsymbol{\tau}_{\boldsymbol{PSS}}$. When $rank(\dot{\boldsymbol{\Theta}}_{\mathbf{P}}) = 0$, $\dot{V}$ vanishes, while the control law remains numerically sound, since $rank(\dot{\boldsymbol{\Theta}}_{\mathbf{P}})^+ = 0^+ = 0$. Thus, (19) holds in all (non-static) cases, and this reveals convergence to $\dot{\boldsymbol{q}}_{\boldsymbol{F_T}} = \mathbf{0}$. However, since the system is non-autonomous, owing to $\boldsymbol{\theta}_{\boldsymbol{d}}(t)$ and $\boldsymbol{q}_{\boldsymbol{d}}(t)$, this precludes direct applicability of LaSalle's Invariance Principle (LP). Despite this, the new Invariance Principle (NIP) [39] circumvents the said issue and simply requires that:

$$\dot{V} = -\dot{\boldsymbol{q}}_{\boldsymbol{F_T}}^T\boldsymbol{\Psi}\dot{\boldsymbol{q}}_{\boldsymbol{F_T}} \leq W \leq 0, \quad (21)$$

where $W = -\dot{\boldsymbol{q}}_{\boldsymbol{F_T}}^T\boldsymbol{\Phi}\dot{\boldsymbol{q}}_{\boldsymbol{F_T}}$, with $\mathbf{0} < \boldsymbol{\Phi} \leq \boldsymbol{\Psi}$. Obtaining W's time derivative subsequently yields:

$$\dot{W} = -2\ddot{\boldsymbol{q}}_{\boldsymbol{F_T}}^T\boldsymbol{\Phi}\dot{\boldsymbol{q}}_{\boldsymbol{F_T}}, \quad (22)$$

which merely reveals that $\dot{W} = 0$, when $\dot{\boldsymbol{q}}_{\boldsymbol{F_T}} = \mathbf{0}$. By differentiating once more, however, it is observed that:

$$\ddot{W} = -2\dddot{\boldsymbol{q}}_{\boldsymbol{F_T}}^T\boldsymbol{\Phi}\dot{\boldsymbol{q}}_{\boldsymbol{F_T}} - 2\ddot{\boldsymbol{q}}_{\boldsymbol{F_T}}^T\boldsymbol{\Phi}\ddot{\boldsymbol{q}}_{\boldsymbol{F_T}}. \quad (23)$$

Thus, $\ddot{W} = 0$ only when $\ddot{\boldsymbol{q}}_{\boldsymbol{F_T}} = \mathbf{0}$, thereby leading to the conclusion that $W \equiv 0$, and $\dot{\boldsymbol{q}}_{\boldsymbol{F_T}} \equiv \mathbf{0}$. It is known that the system's states/trajectories are bounded, given that $\dot{V} \leq 0$ and $V > 0$ [39]. Inserting $\dot{\boldsymbol{q}}_{\boldsymbol{F_T}} = \ddot{\boldsymbol{q}}_{\boldsymbol{F_T}} = \mathbf{0}$ into (3)-(5) yields:

$$\mathbf{K}(\boldsymbol{q} - \boldsymbol{\theta}) + \boldsymbol{\tau}_{\boldsymbol{gq}} - \mathbf{D}\dot{\boldsymbol{\theta}} = \mathbf{0}, \quad (24)$$

$$\mathbf{K}_{\mathbf{P_M}}\boldsymbol{\theta}_{\boldsymbol{E}} + \mathbf{K}_{\mathbf{P_J}}\boldsymbol{q}_{\boldsymbol{E}} = \mathbf{0}. \quad (25)$$

To ensure the existence of a unique equilibrium point, one could utilise the following, link-to-motor position conversion:

$$a_{v1}\boldsymbol{\tau}_{\boldsymbol{gd}} + a_{v0}(\boldsymbol{\tau}_{\boldsymbol{gq}} - \mathbf{D}\dot{\boldsymbol{\theta}}) - \mathbf{K}(\boldsymbol{\theta}_{\boldsymbol{d}} - \boldsymbol{q}_{\boldsymbol{d}}) = \mathbf{0}. \quad (26)$$

The explicit forms of a_{v0}, a_{v1}, and a_{a1} are provided in Appendix B. When $\dot{\boldsymbol{q}}_{\boldsymbol{F_T}} = \ddot{\boldsymbol{q}}_{\boldsymbol{F_T}} = \mathbf{0}$ ($a_{v0} = 1$), one obtains:

$$\boldsymbol{\tau_{gq}} - \mathbf{D}\dot{\boldsymbol{\theta}} - \mathbf{K}(\boldsymbol{\theta_d} - \boldsymbol{q_d}) = \mathbf{0}, \tag{27}$$

since $a_{v0} = 1 - a_{v1}$; thus, $a_{v0} = 1$ when $\dot{\boldsymbol{q}}_{\boldsymbol{F_T}} = \ddot{\boldsymbol{q}}_{\boldsymbol{F_T}} = \mathbf{0}$. Subtracting the above from the reduced link dynamics yields:

$$\mathbf{K}\boldsymbol{q_E} - \mathbf{K}\boldsymbol{\theta_E} = \mathbf{0}. \tag{28}$$

Hence, one finally acquires:

$$\mathbf{T_M}\begin{bmatrix}\boldsymbol{q_E}\\ \boldsymbol{\theta_E}\end{bmatrix} = \begin{bmatrix}\mathbf{K} & -\mathbf{K}\\ \mathbf{K_{P_J}} & \mathbf{K_{P_M}}\end{bmatrix}\begin{bmatrix}\boldsymbol{q_E}\\ \boldsymbol{\theta_E}\end{bmatrix} = \mathbf{0}, \tag{29}$$

which possesses the trivial solution, $\boldsymbol{q_E} = \boldsymbol{\theta_E} = \mathbf{0}$, if $\frac{1}{2}(\mathbf{T_M} + \mathbf{T_M^T}) > \mathbf{0}$, thus proving GAS of $\boldsymbol{q_{eq}}$. When $\mathbf{K}$ is constant (linear stiffness joints), there is no risk of violating *Lemma 1*; thus, to increase the gain range for linear stiffness robots, one may use $\boldsymbol{\tau_{C0}} = \mathbf{J}\ddot{\boldsymbol{\theta}}_{\boldsymbol{e}} - \mathbf{D}\dot{\boldsymbol{q}}_{\boldsymbol{e}} - \mathbf{K}\boldsymbol{q_e}$ and

$$\boldsymbol{\theta_d} = \boldsymbol{q_d} + \mathbf{K}^{-1}(\boldsymbol{\tau_{gq}} - \mathbf{D}\dot{\boldsymbol{\theta}}), \tag{30}$$

which collectively yield:

$$\mathbf{T_{ML}}\begin{bmatrix}\boldsymbol{q_E}\\ \boldsymbol{\theta_E}\end{bmatrix} = \begin{bmatrix}\mathbf{K} & -\mathbf{K}\\ \mathbf{K_{P_J}} & \mathbf{K_{P_M}} + \mathbf{K}\end{bmatrix}\begin{bmatrix}\boldsymbol{q_E}\\ \boldsymbol{\theta_E}\end{bmatrix} = \mathbf{0}. \tag{31}$$

The trivial solution is also the unique solution of this equation, provided that $\frac{1}{2}(\mathbf{T_{ML}} + \mathbf{T_{ML}^T}) > \mathbf{0}$, which is satisfiable even when employing exceedingly low gain values.

D. Higher-Order Terms based on Partial Knowledge of the Link-Side Dynamics Model

Based on the previously provided, link-to-motor position conversion equation, it is possible to compute the higher-order, desired motor velocity and acceleration variables via:

$$\dot{\boldsymbol{\theta}}_{\boldsymbol{d}} = \dot{\boldsymbol{q}}_{\boldsymbol{d}} + \mathbf{K}^{-1}\dot{\boldsymbol{\tau}}_{\boldsymbol{gd}}, \tag{32}$$
$$\ddot{\boldsymbol{\theta}}_{\boldsymbol{d}} = \ddot{\boldsymbol{q}}_{\boldsymbol{d}} + \mathbf{K}^{-1}\ddot{\boldsymbol{\tau}}_{\boldsymbol{gd}}. \tag{33}$$

Since the above equations are applicable when $\dot{\boldsymbol{\theta}}_{\boldsymbol{e}} \neq \mathbf{0}$, one should also consider the more general form of equation (26), based on which the following expressions can be derived:

$$\dot{\boldsymbol{\theta}}_{\boldsymbol{d}} = \dot{\boldsymbol{q}}_{\boldsymbol{d}} + \mathbf{K}^{-1}\left(a_{v1}\dot{\boldsymbol{\tau}}_{\boldsymbol{gd}} + a_{v0}\left(\dot{\boldsymbol{\tau}}_{\boldsymbol{gq}} - \mathbf{D}\ddot{\boldsymbol{\theta}}\right)\right), \tag{34}$$
$$\ddot{\boldsymbol{\theta}}_{\boldsymbol{d}} = \ddot{\boldsymbol{q}}_{\boldsymbol{d}} + \mathbf{K}^{-1}\left(a_{v1}\ddot{\boldsymbol{\tau}}_{\boldsymbol{gd}} + a_{v0}\left(\ddot{\boldsymbol{\tau}}_{\boldsymbol{gq}} - \mathbf{D}\dddot{\boldsymbol{\theta}}\right)\right). \tag{35}$$

If $\mathbf{D}$ and $\mathbf{K}$ are time-varying, then their derivatives are also required; a full derivation is provided in Appendix C. This constitutes one of the main advantages of the proposed PSC approach compared to existing methods, i.e. the fact that it obviates the need for computation of the most cumbersome link dynamics terms, namely $\mathbf{M}$ and $\mathbf{C}$, as well as their higher-order derivatives. Moreover, from a practical viewpoint, the absence of link jerk signals from (5), (34), and (35) renders the proposed scheme safe and efficacious for usage in pHRI applications [36]. This desirable feature materialises in virtue of the PSC approach's ability to rely on Lyapunov functions that depend upon $\dot{\boldsymbol{q}}_{\boldsymbol{F_T}} = [\dot{\boldsymbol{q}}^{\boldsymbol{T}} \;\; \dot{\boldsymbol{\theta}}_{\boldsymbol{e}}^{\boldsymbol{T}}]^{\boldsymbol{T}}$, as opposed to $\dot{\boldsymbol{q}}_{\boldsymbol{F_E}} = [\dot{\boldsymbol{q}}_{\boldsymbol{E}}^{\boldsymbol{T}} \;\; \dot{\boldsymbol{\theta}}_{\boldsymbol{E}}^{\boldsymbol{T}}]^{\boldsymbol{T}}$; vectors similar to the latter are ubiquitous in tracking control of ASRs, as evinced by [13], [18]-[21], [24]. It is worth noting that if the user prefers to avoid activating/deactivating signals using a_{v0} and a_{v1}, then it is entirely possible to employ equation (30) at all times.

E. PSC plus Partial Link-Side Dynamics: Passivity Analysis

Conducting a passivity analysis is crucial, given that the proposed scheme is aimed at tracking, and interaction, control. Repeating the steps adumbrated in Proof 1, while assuming that $\boldsymbol{\tau_e} \neq \mathbf{0}$, yields the relationship:

$$\dot{V} = \dot{Q} = -\dot{\boldsymbol{q}}_{\boldsymbol{F_T}}^{\boldsymbol{T}}\boldsymbol{\Psi}\dot{\boldsymbol{q}}_{\boldsymbol{F_T}} + \dot{\boldsymbol{q}}^{\boldsymbol{T}}\boldsymbol{\tau_e} \leq \dot{\boldsymbol{q}}^{\boldsymbol{T}}\boldsymbol{\tau_e}, \tag{36}$$

thereby leading to satisfaction of a passivity condition [40], which proves that the system interacts stably with any passive, unknown environment [33]. It is worth noting that this condition holds even if a_{vs} is permanently replaced by a_{v1}, since the additional step of inserting $\dot{\boldsymbol{q}}_{\boldsymbol{F_T}} \equiv \mathbf{0}$ into the closed-loop dynamics becomes unnecessary in this case.

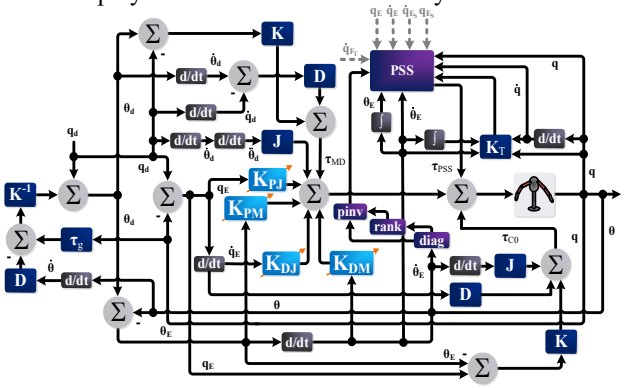

Figure 1. Block diagram of the UMVIC scheme.

As an added benefit, one can produce a passive, closed-loop system by using solely the simplified, link-to-motor variable conversions described by equations (32) and (33) – this is deemed a highly desirable feature since $\boldsymbol{\tau_{gd}}$ is the most straightforwardly computable, link dynamics term (excluding the coupled $\mathbf{K}$ and $\mathbf{D}$ elements).

V. An Uncomplicated Model-Based Scheme for VIC of Nonlinear Stiffness Systems

A. Stable VIC via Partial Knowledge of Link-Side Dynamics

The controllers, and analysis, described thus far have relied upon the assumption that the $\mathbf{K_{P_M}}$ and $\mathbf{K_{P_J}}$ gains remain constant at all times. However, VIC offers numerous benefits in terms of both tracking, and interactional, performance [6][8][30]. In general, PSC enables stable VIC, although this necessitates an iota of modifications w.r.t to the scheme presented in the previous section. Firstly, when using $\mathbf{K_{P_{Mt}}} = \mathbf{K_{P_M}}(t)$, and $\mathbf{K_{P_{Jt}}} = \mathbf{K_{P_J}}(t)$, *Lemma 1* is valid only if impedance modulations are *momentarily* suspended ($\dot{\mathbf{K}}_{\mathbf{P_M}} = \dot{\mathbf{K}}_{\mathbf{P_J}} = \mathbf{0}$) when $\dot{\boldsymbol{\theta}}_{\boldsymbol{E}} = \mathbf{0}$. The PSS also requires some amendment, since residual terms appear in $\dot{V}$ due to VIC.

Theorem 2: The closed-loop system comprising equations (3)-(5), with $\mathbf{K_{P_M}}(t)$ and $\mathbf{K_{P_J}}(t)$, possesses a GAS equilibrium point at $\boldsymbol{q_{eq}} = \begin{bmatrix}\dot{\boldsymbol{q}}^T & \dot{\boldsymbol{\theta}}_E^T & \boldsymbol{q}_{E_S}^T & \boldsymbol{\theta}_E^T\end{bmatrix} = \mathbf{0}$, when $\boldsymbol{\tau_e} = \mathbf{0}$, provided that $\dot{\mathbf{K}}_{\mathbf{P_M}} = \dot{\mathbf{K}}_{\mathbf{P_J}} = \mathbf{0}$ when $\dot{\boldsymbol{\theta}}_E = \mathbf{0}$.

Proof 2: Considering the same Lyapunov function as before, and computing its time derivative – followed by similar simplifications – yields the result:

$$\dot{V} = -\dot{\boldsymbol{q}}_{F_T}^{\boldsymbol{T}}\boldsymbol{\Psi}\dot{\boldsymbol{q}}_{F_T} + \tfrac{1}{2}\boldsymbol{\theta}_E^{\boldsymbol{T}}\dot{\mathbf{K}}_{\mathbf{P_M}}\boldsymbol{\theta}_E + \tfrac{1}{2}\boldsymbol{q}_{E_S}^{\boldsymbol{T}}\dot{\mathbf{K}}_{\mathbf{P_J}}\boldsymbol{q}_{E_S}. \quad (37)$$

Hence, in order to eliminate the new terms appearing on the RHS, one ought to define the following PSS:

$$p_{sse} = p_{ss} - \frac{\boldsymbol{\theta}_E^{\boldsymbol{T}}\mathbf{K_{P_M}}\boldsymbol{\theta}_E}{2} - \frac{\boldsymbol{q}_{E_S}^{\boldsymbol{T}}\dot{\mathbf{K}}_{\mathbf{P_J}}\boldsymbol{q}_{E_S}}{2}, \quad (38)$$

which would again result in $\dot{V} = -\dot{\boldsymbol{q}}_{F_T}^{\boldsymbol{T}}\boldsymbol{\Psi}\dot{\boldsymbol{q}}_{F_T}$. This adapted controller is dubbed the uncomplicated-model-based VIC (UMVIC) scheme (Fig. 1). It is worth reemphasising that impedance increases are to be *momentarily* suspended when $\dot{\boldsymbol{\theta}}_E = \mathbf{0}$; a condition that guarantees applicability of *Proof 1's* (and *Lemma 1's*) conclusions to this scenario.

B. VIC based on Partial Knowledge of the Link-Side Dynamical Model & Nonlinear Stiffnesses

Using the proposed PSC approach, it is possible to stably perform VIC on nonlinear stiffness robots [18][20][24]. As a matter of fact, the only alteration that is required, as regards the schemes presented thus far, is replacement of $\mathbf{K}$ with $\mathbf{K}(t)$—analogous modifications should also be carried out to the motor-to-link conversion equations. To expand the impedance value range when using $\mathbf{K}(t)$, one can introduce a new switching variable, a_{vc} (Appendix B), that is activated when $\dot{\boldsymbol{\theta}}_E = \mathbf{0}$ (or $\dot{\boldsymbol{\theta}}_E \neq \mathbf{0}$) and $\dot{\boldsymbol{q}}_{F_T} \not\equiv \mathbf{0}$, and is deactivated only when $\dot{\boldsymbol{\theta}}_E = \mathbf{0}$ and $\dot{\boldsymbol{q}}_{F_T} \equiv \mathbf{0}$. Thus, one could use:

$$\boldsymbol{\tau_{C0}} = \mathbf{J}\ddot{\boldsymbol{\theta}}_e - \mathbf{D}\dot{\boldsymbol{q}}_e + \mathbf{K}(a_{vc}\boldsymbol{\theta}_e - \boldsymbol{q}_e). \quad (39)$$

Omitting a painstaking analysis for the sake of brevity, this combination of signals yields (31), and therefore $\boldsymbol{\theta}_E = \boldsymbol{q}_E = \mathbf{0}$. In theory, this enables usage of exceedingly low gains. Equation (39) does not represent the full control signal, but merely a portion of it; the full control input signal is represented via equation (5), where $\boldsymbol{\tau_{C0}}$ is just one of numerous components – the purpose of $\boldsymbol{\tau_{C0}}$ is to guarantee stability by eliminating any residual elements appearing when $\dot{\boldsymbol{\theta}}_E = \mathbf{0}$. The overall control system's block diagram is illustrated in Fig. 1. Many of the matrices and calculations required to produce $\boldsymbol{\tau}_{PSS}$ have been omitted for clarity, as these are assumed to be contained within the PSS block.

C. Partial Link-Side Dynamical Modelling, Nonlinear Stiffness, VIC Passivity

In contrast to the stability analysis results, passivity is ensured even when the reduced link-to-motor variable conversions are permanently used. However, for the passivity results to hold, one must again ensure that impedance *increases* are *momentarily* suspended when $\dot{\boldsymbol{\theta}}_E = \mathbf{0}$, otherwise the sign of:

$$\dot{Q} = -\dot{\boldsymbol{q}}^{\boldsymbol{T}}\boldsymbol{\Psi}_{\mathbf{11}}\dot{\boldsymbol{q}} + \frac{\boldsymbol{\theta}_E^{\boldsymbol{T}}\mathbf{K_{P_M}}\boldsymbol{\theta}_E}{2} + \frac{\boldsymbol{q}_{E_S}^{\boldsymbol{T}}\dot{\mathbf{K}}_{\mathbf{P_J}}\boldsymbol{q}_{E_S}}{2} + \dot{\boldsymbol{q}}^{\boldsymbol{T}}\boldsymbol{\tau_e} \leq \dot{\boldsymbol{q}}^{\boldsymbol{T}}\boldsymbol{\tau_e}, \quad (40)$$

will be indeterminate; $\boldsymbol{\Psi}_{\mathbf{11}}$ is the upper left block of $\boldsymbol{\Psi}$. If, however, $\dot{\boldsymbol{\theta}}_E = \mathbf{0}$ and $\boldsymbol{q}_{E_S} = \boldsymbol{\theta}_E = \mathbf{0}$, then even impedance *increases* are permitted. In general, designing a passivating controller is a simpler task, since it obviates usage of the NIP.

D. Gain-Independent Saturation Prevention Method

To avoid imposing undesirable gain modulations, and thus limiting the user's ability to realise a predetermined impedance profile, the following PSS is proposed:

$$p_{sl} = p_{sse} - \psi^2\ddot{\boldsymbol{q}}_{F_T}^{\boldsymbol{T}}\dot{\boldsymbol{q}}_{F_T} - \dot{\psi}\cdot\psi\cdot\dot{\boldsymbol{q}}_{F_T}^{\boldsymbol{T}}\dot{\boldsymbol{q}}_{F_T}, \quad (41)$$

where ψ denotes a user-modulated scalar. The following, adapted Lyapunov function can then be considered:

$$V = \frac{\dot{\boldsymbol{q}}_{F_T}^{\boldsymbol{T}}\mathbf{M_T}\dot{\boldsymbol{q}}_{F_T}}{2} + \frac{\boldsymbol{\theta}_E^{\boldsymbol{T}}\mathbf{K_{P_M}}\boldsymbol{\theta}_E}{2} + \frac{\boldsymbol{q}_{E_S}^{\boldsymbol{T}}\mathbf{K_{P_J}}\boldsymbol{q}_{E_S}}{2} + \frac{\psi^2\dot{\boldsymbol{q}}_{F_T}^{\boldsymbol{T}}\dot{\boldsymbol{q}}_{F_T}}{2}. \quad (42)$$

Additional details are omitted, since similar saturation prevention methods can be applied to all PSC-based schemes, as delineated in [20][26][27]. Impedance modulations may be performed unrestrainedly, without impinging on stability.

VI. Experiments Involving a Flexible-Joint Robot: Tracking, pHRI, & a Button-Pressing Task

A. Experimental Setup

The Rethink Robotics Baxter is a bimanual robot that stands at a height of approximately 1.83 m, and weighs 138.8 kg, when mounted on its custom pedestal. Further, it is a flexible-joint robot (ASR), given that its arms are powered through a combination of DC motors and SEAs. Baxter's shoulder/elbow, and wrist, joints possess flexure stiffness values of 843, and 250 Nm/rad, respectively [40]. The experimental setup comprises an Intel Core i7-10700 @ 2.9 GHz desktop PC, running Robot Operating System (ROS) Melodic, via Ubuntu 18.04.5 LTS (Bionic Beaver). The Baxter's low-level joint controller executes at a rate of 1ms, while the Python script used to implement the UMVIC scheme runs at a rate of approximately 0.5ms, thus being suitable for real-time implementation.

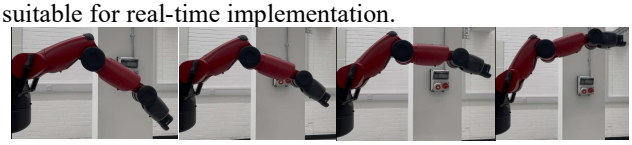

Figure 2. Trajectory-tracking control using link position references.

B. Flexible-Joint Arm Tracking during Free Motion

The tracking experiments (Fig. 2) entail controlling the Baxter robot's left arm via the UMVIC scheme, which is supplied with two different, sinusoidal, link-position trajectories: a slow one (Figs. 3-4), and a faster one (Figs. 5-6). Figs. 3 and 5 reveal that the arm's links ($\boldsymbol{q}$) are able to accurately track the commanded references ($\boldsymbol{q_d}$). It is worth noting that s_1, e_1,

and w_1 denote the sagittal shoulder, elbow, and wrist link positions ($\boldsymbol{q}$), respectively, while s_0, e_0, w_0, and w_2 signify the remaining roll/yaw joints. Figure 4 shows that after moving to a homing position, the arm's proportional gains ($\mathbf{K_{P_J}}$) are increased and remain constant throughout (the same impedance profile is used for the "faster" experiment). Fig. 6 also demonstrates that the PSS is confined to evolving within user-defined bounds (p_d). Fig. 7 compares the tracking performance of the UMVIC scheme to that of a controller based on a full model of the system; the scheme introduced in [20] is employed for this comparative analysis, as it is the only one reported in literature suited to VIC of ASRs. Identical gains were used in both cases, with the only difference being the superimposition of the link dynamics terms (link-to-motor position conversions), and some auxiliary signals, in the case of the controller described in [20]. Fig. 7 reveals that these schemes perform almost identically in terms of position control accuracy, despite the increased complexity of [20].

C. pHRI Experiments Involving a Flexible-Joint Robot Arm

The first pHRI experiment, which is depicted in Fig. 8, attempts to showcase that – when controlled using the proposed scheme – the Baxter robot's left arm is capable of tracking a sinusoidal, joint-space position trajectory, while physically interacting with a human user. Figs. 9-13 reveal that once the robot's arm comes into contact with the user, and a predefined threshold is exceeded, the wrist and elbow position gains decrease abruptly, thereby increasing the position error momentarily. However, tracking performance is recovered once the effects of the external impacts have subsided, thus demonstrating that the proposed controller enables the arm to simultaneously track trajectories, and interact with its environment. The predefined threshold is triggered by the real-time value of the external contact force vector's norm and is set to a magnitude that exceeds the wrench feedback's noise levels (despite being smoothed using a 60-sample averaging filter). The physical experiment during which this data was recorded can be viewed in the video attachment. The gain values ($\mathbf{K_{P_J}}$) pertaining to Figs. 9 and 12 are contained in Figs. 10 and 13, respectively. Also, Fig. 11 plots the contact wrenches measured during low-speed tracking, Fig. 14 displays the

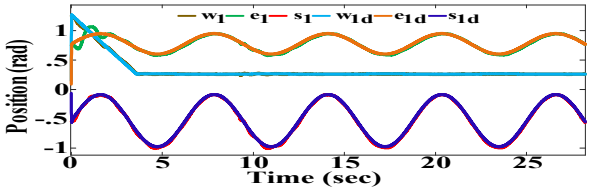

Figure 3. Tracking a "slow" reference: e_1 and s_1 track sinusoidal, joint position references, while w_1 is ramped to a constant position reference.

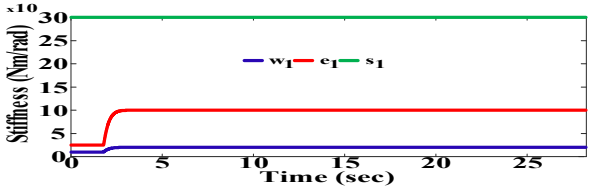

Figure 4. Tracking a "slow" reference: the e_1 and w_1 gains are increased, while the s_1 gains remain constant.

accompanying power-shaping torque values, and Fig. 15 shows the ψ variable's evolution. It is noteworthy that all experiments involve usage of identical, referential link-position trajectories, and vertical, blue dotted lines are used to denote the moments of impact between the Baxter and the environment.

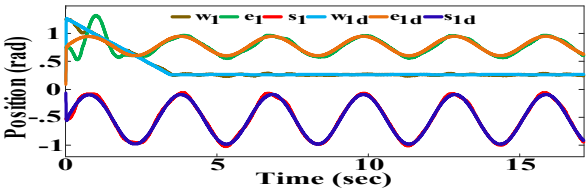

Figure 5. Tracking a "faster" reference: e_1 and s_1 track sinusoidal, link position references, while w_1 is ramped to a constant position reference.

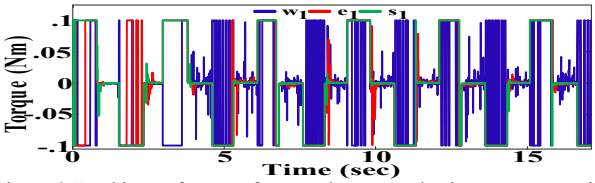

Figure 6. Tracking a "faster" reference: the power-shaping torques pertaining to the w_1, e_1, and s_1 joints are bounded within user-defined limits.

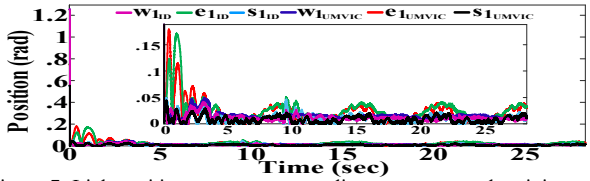

Figure 7. Link position errors corresponding to w_1, e_1, and s_1 joints when using UMVIC versus using the model-based controller described in [20].

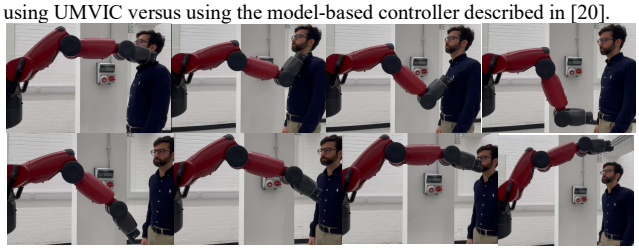

Figure 8. pHRI experiment (upper row: arm moving downwards while interacting with the user; lower row: arm moving upwards in "free motion").

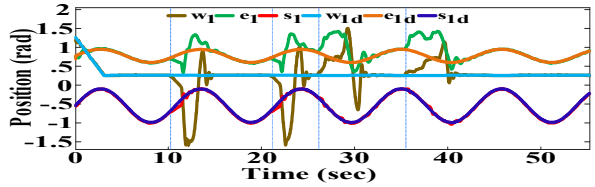

Figure 9. UMVIC "Low Speed" pHRI: e_1 and s_1 track sinusoidal, link position references, while also interacting with a human user.

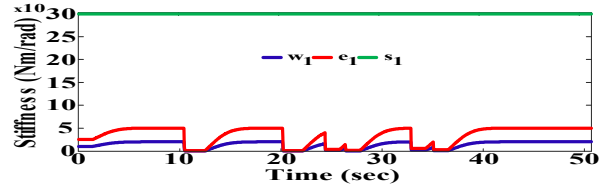

Figure 10. UMVIC "Low Speed" pHRI: the e_1 and w_1 gains are decreased once the robot's arm comes into contact with a human user.

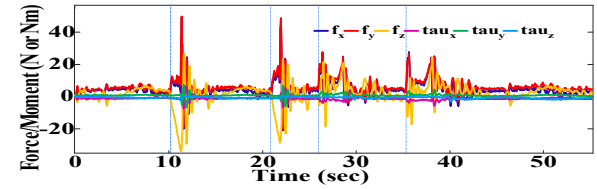

Figure 11. UMVIC "Low Speed" pHRI: contact wrench values during pHRI.

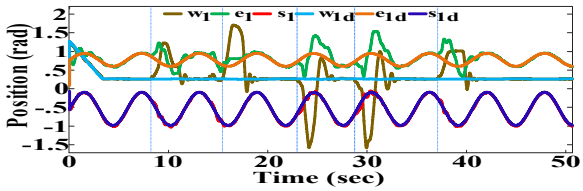

Figure 12. UMVIC "Higher Speed" pHRI: e_1 and s_1 track sinusoidal, link position references, while also interacting with a human user.

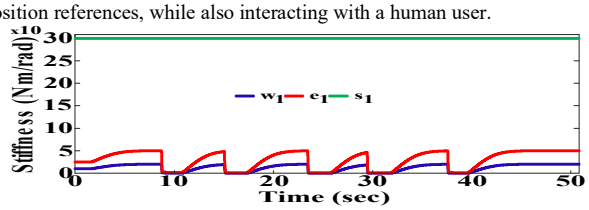

Figure 13. UMVIC "Higher Speed" pHRI: the e_1 and w_1 gains are decreased once the robot's arm comes into contact with a human user.

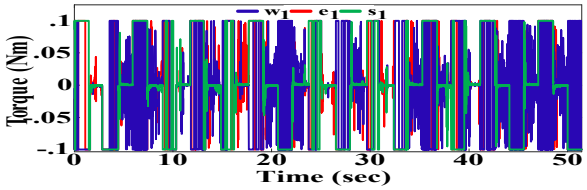

Figure 14. UMVIC "Higher Speed" pHRI: the power-shaping torques pertaining to the w_1, e_1, and s_1 joints are bounded within user-defined limits.

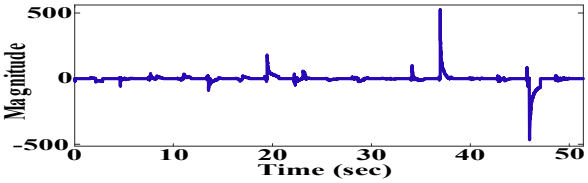

Figure 15. UMVIC "Higher Speed" pHRI: evolution of the ψ variable.

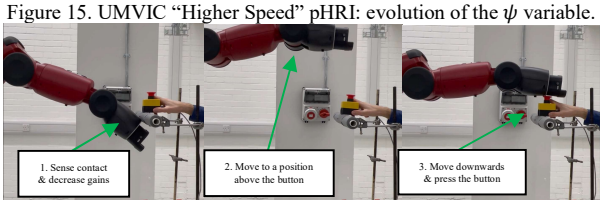

Figure 16. Illustration of the aim of the experiment.

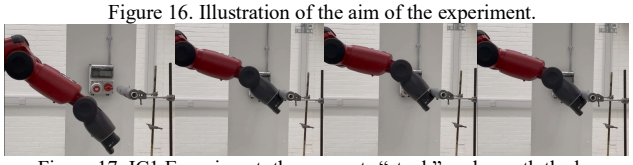

Figure 17. IC1 Experiment: the arm gets "stuck" underneath the bar.

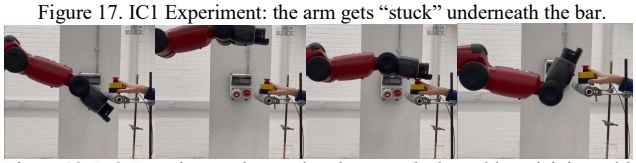

Figure 18. IC2 Experiment: the arm brushes past the bar, although it is unable to produce the force required to press the button.

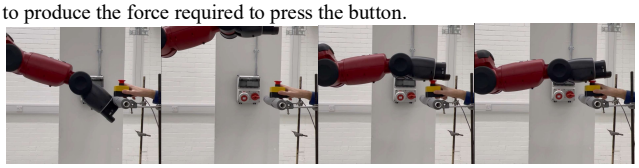

Figure 19. IC3 Experiment: the arm brushes past the bar and is also able to produce the force required to press the button.

D. Interacting with a Horizontal Bar & Pressing a Button

For the second set of physical interaction experiments, illustrated via Figs. 16-19, the robot is assigned a specific task that it needs to execute via the UMVIC scheme: the aim is for the robotic arm to move upwards towards a horizontal bar, sense the contact, activate VIC to negotiate the obstacle, and once the wrist has moved to a Cartesian position above the bar, activate a new trajectory to move the wrist towards an emergency button. Figs. 20-21 pertain to trials conducted using a fixed-gain version of UMVIC, namely IC1; Figs. 22-23 relate to trials performed using the UMVIC scheme with an exceedingly sensitive force trigger, namely IC2; Figs. 24-25 are extracted during trials preformed when using the UMVIC scheme with a less sensitive trigger, namely IC3. When employing IC1, it is evident from Fig. 20 that the robot's arm is unable to move past the horizontal bar, owing to the constant, high $\mathbf{K_{P_J}}$ gains (Fig. 21). The second physical interaction experiment – involving IC2 – reveals that the robot's arm is capable of brushing past the horizontal bar, albeit being incapable of pressing the button, since the gains are decreased before the required force is generated by the wrist/arm – a clearer illustration is provided in the video.

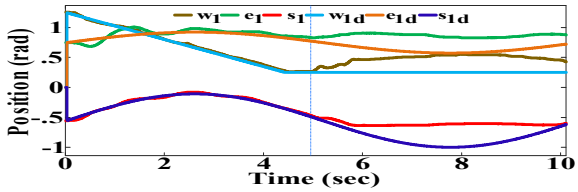

Figure 20. IC1 Experiment: w_1, e_1 and s_1 are unable to continue following the relevant references after coming into contact with the horizontal bar.

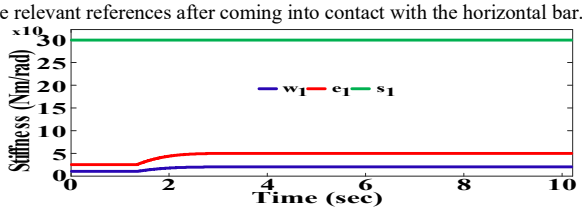

Figure 21. IC1 Experiment: the w_1 and e_1 link position gains ($\mathbf{K_{P_J}}$) are ramped to a set of constant values.

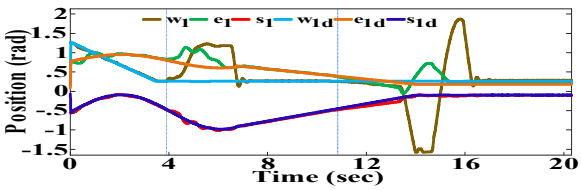

Figure 22. IC2 Experiment: w_1, e_1 and s_1 deviate from their reference values momentarily, once they come into contact with the horizontal bar and button.

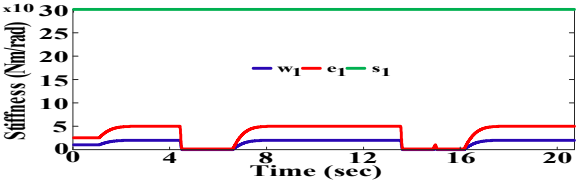

Figure 23. IC2 Experiment: the w_1 and e_1 link position gain values decrease upon impact with the horizonal bar, as well as with the emergency button.

Finally, the third experiment – pertaining to IC3 – demonstrates that the robot is capable of brushing past the bar and pressing the emergency button (which coincidentally deactivates its power supply), as shown in the accompanying video. Comparing Figs. 20, 22, and 24 to one another reveals that when using IC1, the robot has no control over the

interaction between itself and the environment. Although IC2 does endow the robot with an indirect force control capability, its impedance switching settings preclude applying the right amount of force onto the button. Contrarily, IC3 demonstrates that by using a less sensitive impedance switching trigger, the robot can brush past the horizontal bar, as well as apply the "correct" amount of force required to press the button, as demonstrated via the accompanying video file. It is worth clarifying that for all the experiments, i.e. IC1-IC3, the exact same, predetermined, link-position trajectories are employed, and these are not modified at any phase during the robot's operation.

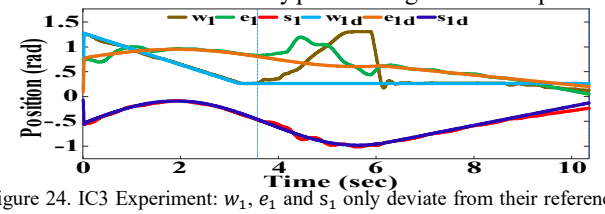

Figure 24. IC3 Experiment: w_1, e_1 and s_1 only deviate from their reference values momentarily, once they come into contact with the horizontal bar.

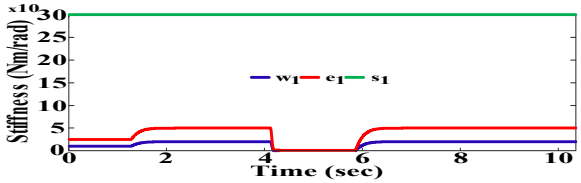

Figure 25. IC3 Experiment: the w_1 and e_1 link position gains decrease upon impact with the horizonal bar and remain constant while pressing the button.

E. Interacting with a Horizontal Bar at Different Speeds: Effect of Including & Excluding Link Jerk Feedback

Four sets of experiments (HBI1-HBI4) were conducted to demonstrate the benefit/s of using the proposed UMVIC scheme, which excludes link-jerk feedback, over existing trajectory-tracking controllers for flexible-joint robots that require usage of link jerk feedback. Since the experiments involved VIC, the controller used for comparative purposes is that introduced in [20], which enables stable VIC.

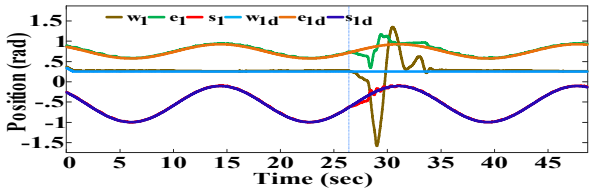

Figure 26. HBI1 Experiment: Link position responses recorded when brushing past a horizontal bar at "low" speed using the UMVIC scheme.

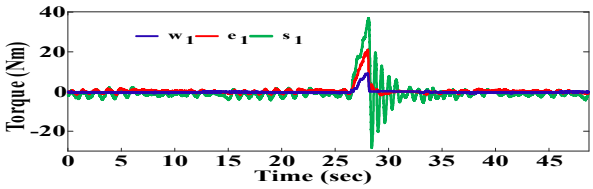

Figure 27. HBI1 Experiment: Control torque inputs recorded when brushing past a horizontal bar at "low" speed using the UMVIC scheme.

The rationale is that comparing the UMVIC scheme to a trajectory-tracking controller for flexible-joint robots that does not offer VIC stability guarantees, would be a technically unsound choice. These experiments revolve around execution of the same sinusoidal trajectory as that used for the tracking experiments in VI. B, while relying on VIC to brush past the horizontal bar; no button-pressing is involved in this case. HBI1 and HBI2 entail execution of link position trajectories using the UMVIC scheme, while HBI3 and HBI4 involve execution of the same trajectories using the controller proposed in [20], which requires link-jerk feedback. Further, HBI1 and HBI3 involve usage of "slow" trajectories (Figs. 26 & 30), while HBI2 and HBI4 revolve around faster trajectories (Figs. 28 & 32). Figs. 26-29 reveal that the proposed UMVIC scheme remains unaffected by trajectory speed increases, even during impact. Contrariwise, Figs. 30-33 demonstrate that using the link-jerk feedback scheme introduced in [20] induces input torque spikes, and saturation, when the trajectory speed is increased, and the robot interacts with the environment.

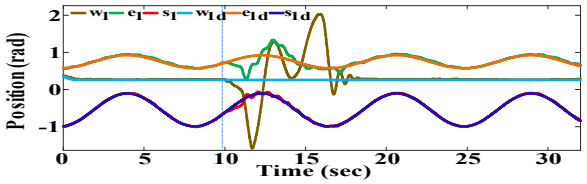

Figure 28. HBI2 Experiment: Link position responses recorded when brushing past a horizontal bar at higher speed using the UMVIC scheme.

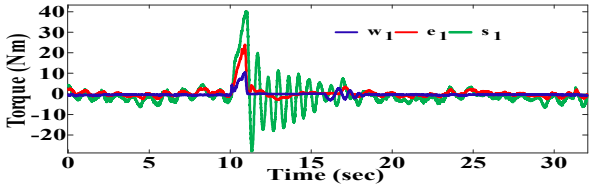

Figure 29. HBI2 Experiment: Control torque inputs recorded when brushing past a horizontal bar at higher speed using the UMVIC scheme.

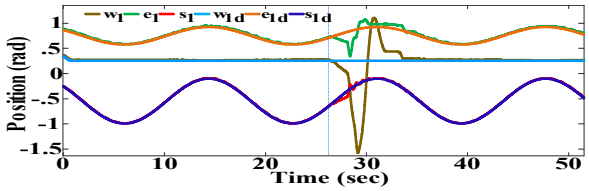

Figure 30. HBI3 Experiment: Link position responses when brushing past a horizontal bar at "low" speed using a link-jerk-feedback scheme.

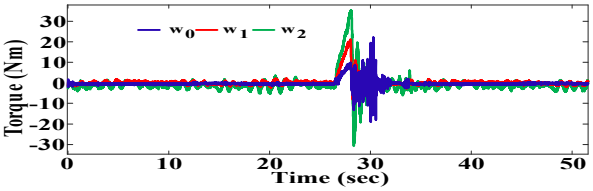

Figure 31. HBI3 Experiment: Control torque inputs recorded when brushing past a horizontal bar at "low" speed using a link-jerk-feedback scheme.

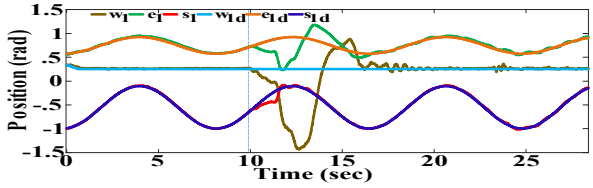

Figure 32. HBI4 Experiment: Link position responses when brushing past a horizontal bar at higher speed using a link-jerk-feedback scheme.

This effect is epitomised by Fig. 33, which displays an input torque spike at the moment of impact between the Baxter's arm and the horizontal bar – this torque spike far exceeds the

joint torque limits of the wrist joint, *w1*. Fig. 32 reveals that the system is unable to damp out the post-impact oscillations, resulting in frequent saturation of the wrist joint torque input, in contrast to the results contained in Figs. 26, 28, and 30.

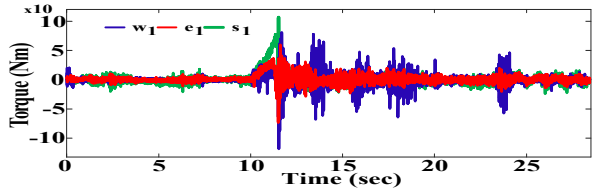

Figure 33. HBI4 Experiment: Control torque inputs recorded when brushing past a horizontal bar at higher speed using a link-jerk-feedback scheme.

The wrist joint stuttering/chattering arising from torque input saturation is clearly showcased in the video attachment.

VII. Discussion of Controller Limitations

Although the UMVIC scheme is less dependent on model-based terms, as compared to other, existing trajectory-tracking controller designs for flexible-joint robots (with stability guarantees), it still falls short of solving the tracking problem in a model-free manner while offering stability guarantees, e.g. global asymptotical stability. Moreover, obtaining a highly accurate motor dynamics model might be challenging, especially if the robot exhibits manifold nonlinear stiffness, damping, friction, and backlash phenomena that may be time- and temperature-dependent; this requirement is ultimately determined by the nature of the robotic hardware. At any rate, the accuracy of the motor dynamics model will inevitably dictate the performance of the UMVIC scheme, especially since nonlinear impedances give rise to a need for first and second derivatives of the **K** and **D** matrices. Another means of improving tracking (but not interactional) performance is via usage of integral action on the link position; however, this exceeds the current work's scope and will therefore constitute the topic of future study. Although the proposed method offers stability guarantees when using impedance gains modulated at arbitrary rates, whilst also avoiding usage of link jerk signals, it does not explicitly deal with how these gains should be selected – this topic is addressed extensively in [28][29][41][42][43].

VIII. Conclusion

This work presents a novel control scheme, namely UMVIC, that is capable of endowing ASRs – comprising both linear and nonlinear passive stiffness elements – with the ability to simultaneously track trajectories, and safely interact with their environments; this is achieved, for the first time, in the absence of the link inertia and Coriolis matrices. In addition to enabling unconstrained VIC (with stability guarantees) for improved interaction, the proposed UMVIC scheme permits usage of non-collocated state feedback elements for enhanced tracking performance. Most importantly, however, the aforementioned features are effectuated by means of a simple control scheme that relies on partial knowledge of the link-side dynamics model, given that it obviates the need for computation of the link inertia matrices, Coriolis/centrifugal terms, and any variables exceeding the third-order derivative of the motor position vector; this stands in stark contrast to analogous schemes. Experimental data extracted from the Baxter robot demonstrates the usefulness of VIC in practical applications requiring both interaction and tracking control. Moreover, the experiments corroborate this work's theoretical results, by means of demonstrating stable execution of all the relevant, practical tasks.

Appendix A

Inserting $\boldsymbol{q_{eq}} = \begin{bmatrix}\dot{\boldsymbol{q}}^T & \dot{\boldsymbol{\theta}}_{\boldsymbol{E}}^T & \boldsymbol{q}_{\boldsymbol{E_S}}^T & \boldsymbol{\theta}_{\boldsymbol{E}}^T\end{bmatrix} = \mathbf{0}$ into the system comprising equations (3)-(5) and (27) yields:

$$\mathbf{M}(\boldsymbol{q})\ddot{\boldsymbol{q}} = \mathbf{0}, \tag{43}$$

$$\mathbf{0} = \mathbf{K}_{\mathbf{P_{Mt}}}\boldsymbol{\theta}_{\boldsymbol{E}} + \mathbf{K}_{\mathbf{P_{Jt}}}\boldsymbol{q}_{\boldsymbol{E}}. \tag{44}$$

Acknowledging the fact that $\mathbf{M}(\boldsymbol{q}) = constant$, owing to $\dot{\boldsymbol{q}} = \mathbf{0}$, then by virtue of $\mathbf{M}$'s invertibility, $\ddot{\boldsymbol{q}} = \mathbf{0}$. Since the dynamics vanishes at this point, then it corresponds to the system's origin; this can also be cross verified by inserting $\boldsymbol{q_{eq}} = \mathbf{0}$ into V, which yields $V = 0$. In fact, this is the only point at which $V = 0$. An interesting case arises when $\dot{\boldsymbol{q}} \neq \mathbf{0}$, $\boldsymbol{\theta_E} = \mathbf{0}$, and $\dot{\boldsymbol{\theta}}_{\boldsymbol{e}} = \mathbf{0}$ (*Lemma 1*), since the controller instantaneously enforces $\boldsymbol{q} = const.$, and $\dot{\boldsymbol{q}} = \mathbf{0}$, due to $a_{vs} = 0$. Plugging these values into V yields:

$$V = \frac{1}{2}\boldsymbol{q}^T\mathbf{K}_{\mathbf{P_J}}\boldsymbol{q}, \tag{45}$$

$$\dot{V} = \dot{\boldsymbol{q}}^T\mathbf{K}_{\mathbf{P_J}}\boldsymbol{q}. \tag{46}$$

$\dot{V}$ always vanishes since $\dot{\boldsymbol{q}} = \mathbf{0}$, although V only vanishes if $\boldsymbol{q} = \mathbf{0}$. However, this again corresponds to the origin given that $\boldsymbol{q_{eq}} = \begin{bmatrix}\dot{\boldsymbol{q}}^T & \dot{\boldsymbol{\theta}}_{\boldsymbol{E}}^T & \boldsymbol{q}_{\boldsymbol{E_S}}^T & \boldsymbol{\theta}_{\boldsymbol{E}}^T\end{bmatrix} = \begin{bmatrix}\dot{\boldsymbol{q}}^T & \dot{\boldsymbol{\theta}}_{\boldsymbol{E}}^T & -\boldsymbol{q}^T & \boldsymbol{\theta}_{\boldsymbol{E}}^T\end{bmatrix} = \mathbf{0}$, when $a_{vs} = 0$, thereby producing:

$$-\mathbf{D}\dot{\boldsymbol{\theta}} - \mathbf{K}\boldsymbol{\theta} = \boldsymbol{\tau}_{\boldsymbol{gq}} - \mathbf{D}\dot{\boldsymbol{\theta}} - \mathbf{K}(\boldsymbol{\theta_d} - \boldsymbol{q_d}), \tag{47}$$

which – given that $\boldsymbol{\tau}_{\boldsymbol{gq}}(\mathbf{0}) = \mathbf{0}$ – reduces to:

$$\mathbf{K}\boldsymbol{q_d} = \mathbf{0}, \tag{48}$$

This merely confirms that $\boldsymbol{q} = \mathbf{0}$ when $\boldsymbol{q_d} = \mathbf{0}$ (and vice versa); in other words, that $\boldsymbol{q_E} = \mathbf{0}$.

Appendix B

The scalar term, a_{v1}, is constructed as follows:

$$a_{v1} = \dot{\boldsymbol{\theta}}_{\boldsymbol{e}}^T\dot{\boldsymbol{\Theta}}_{\mathbf{P}}\boldsymbol{I_R}, \tag{49}$$

while $a_{v0} = 1 - a_{v1}$. Additionally, the a_{a1} scalar is given as:

$$a_{a1} = \dot{\boldsymbol{q}}^T\mathbf{Q}_{\mathbf{V_A}}\boldsymbol{I}_{\boldsymbol{V_A}}, \tag{50}$$

where $\mathbf{Q}_{\mathbf{V_A}} = diag(\dot{\boldsymbol{q}})^+ \in \mathbb{R}^{n\times n}$, and $\boldsymbol{I}_{\boldsymbol{V_A}} = [1 \dots 1_n]^{\boldsymbol{T}} \cdot rank\left(\mathbf{Q}_{\mathbf{V_A}}\right)^+$. Hence, $a_{a1} = 1$ when $\dot{\boldsymbol{q}} \neq \mathbf{0}$, and $a_{a1} = 0$ when $\dot{\boldsymbol{q}} = \mathbf{0}$. Moreover, the scalar $a_{vc} = (a_{v0} - 1 - a_{vst})(a_{v0} - 1 - a_{vst})^+$, where:

$$a_{vst} = \begin{bmatrix}\ddot{\boldsymbol{q}}_{\boldsymbol{F_T}}^T & \dot{\boldsymbol{q}}_{\boldsymbol{F_T}}^T\end{bmatrix} \cdot \mathbf{Q}_{\mathbf{F_T}}\boldsymbol{I}_{\boldsymbol{F_T}}, \tag{51}$$

with $\mathbf{Q}_{\mathbf{F_T}} = diag\left(\ddot{\boldsymbol{q}}_{\boldsymbol{F_T}}, \dot{\boldsymbol{q}}_{\boldsymbol{F_T}}\right)^{+}$, $\boldsymbol{I}_{\boldsymbol{F_T}} = [1 \dots 1_{4n}]^{T} \cdot rank\left(\mathbf{Q}_{\mathbf{F_T}}\right)^{+}$.

APPENDIX C

If **K** and **D** contain time-varying elements, then:

$$\dot{\boldsymbol{\theta}}_d = \dot{\boldsymbol{q}}_d + \mathbf{K}^{-1}\big(a_{v1}\dot{\boldsymbol{\tau}}_{gd} + a_{v0}\dot{\boldsymbol{\tau}}_{gq} - a_{v0}\dot{\mathbf{D}}\dot{\boldsymbol{\theta}} - a_{v0}\mathbf{D}\ddot{\boldsymbol{\theta}} - \dot{\mathbf{K}}\boldsymbol{\theta}_d + \dot{\mathbf{K}}\boldsymbol{q}_d\big), \quad (52)$$

$$\ddot{\boldsymbol{\theta}}_d = \ddot{\boldsymbol{q}}_d + \mathbf{K}^{-1}\big(a_{v1}\ddot{\boldsymbol{\tau}}_{gd} + a_{v0}\big(\ddot{\boldsymbol{\tau}}_{gq} - \ddot{\mathbf{D}}\dot{\boldsymbol{\theta}} - 2\dot{\mathbf{D}}\ddot{\boldsymbol{\theta}} - \mathbf{D}\dddot{\boldsymbol{\theta}}\big) - \ddot{\mathbf{K}}\boldsymbol{\theta}_d - 2\dot{\mathbf{K}}\dot{\boldsymbol{\theta}}_d + \ddot{\mathbf{K}}\boldsymbol{q}_d + 2\dot{\mathbf{K}}\dot{\boldsymbol{q}}_d\big), \quad (53)$$

in view of the fact that a_{v1} and a_{v0} switch between binary values (0 and 1 only) instantaneously, and their derivatives are therefore assumed to be zero. Even without making this assumption, it is still possible to compute $\dot{\boldsymbol{\theta}}_d$ and $\ddot{\boldsymbol{\theta}}_d$ via the above expressions, as they are user-defined terms that do not violate any of the conditions stipulated by the NIP. If the user opts for $\boldsymbol{\theta_d} = \boldsymbol{q_d} + \mathbf{K}^{-1}\left(\boldsymbol{\tau}_{gq} - \mathbf{D}\dot{\boldsymbol{\theta}}\right)$ instead (equation (30)), while **K** and **D** are time-varying, then it is possible to use expressions (52), (53) after inserting $a_{v1} = 0$, $a_{v0} = 1$.

REFERENCES

[1] B. Siciliano, O. Khatib, *Springer Handbook of Robotics*, 2 ed., 2016.

[2] N. Hogan, "Impedance Control: An Approach to Manipulation," *American Control Conference, pp. 304-313, 1984.*

[3] N. Hogan, "On the stability of manipulators performing contact tasks," *IEEE Journal on Robotics and Automation, pp. 677-686, 1988.*

[4] B. Hannaford, J. -H. Ryu, "Passive Hierarchical Impedance Control via Energy Tanks," *IEEE Transactions on Robotics and Automation, vol. 18, no. 1, pp. 1-10, 2002.*

[5] D. Lee, K. Huang, "Passive-Set-Position-Modulation Framework for Interactive Robotic Systems," *IEEE Transactions on Robotics, vol. 26, no. 2, pp. 354-369, 2010.*

[6] F. J. Abu-Dakka, M. Saveriano, "Variable Impedance Control and Learning—A Review," *Frontiers in Robotics and AI, vol. 7, 2020.*

[7] C. Zeng et al., "A Unified Parametric Representation for Robotic Compliant Skills with Adaptation of Impedance and Force," *IEEE/ASME Transactions on Mechatronics, vol. 27, no.2, pp.623-633, 2022.*

[8] J. Buchli et al., "Learning variable impedance control," *The International Journal of Robotics Research, vol. 30, no. 7, pp. 820-833, 2011.*

[9] G. Pratt, M. Williamson, "Series Elastic Actuators," *IEEE/RSJ International Conference on Intelligent Robots and Systems, pp. 399-406, 1995.*

[10] P. Qi et al., "A Novel Continuum Manipulator Design Using Serially Connected Double-Layer Planar Springs," *IEEE/ASME Transactions on Mechatronics, vol. 21, no.3, pp. 1281-1292, 2016.*

[11] R. Mengacci et al., "On the motion/stiffness decoupling property of articulated soft robots with application to model-free torque iterative learning control," *The International Journal of Robotics Research, vol. 40, no. 1, pp. 348-374, 2021.*

[12] H. Lee, S. Oh, "Series Elastic Actuators-Driven Parallel Robot with Wide-Range Impedance Realization for Balance Assessment and Training," *IEEE/ASME Transactions on Mechatronics, vol. 27, no. 6, 2022.*

[13] S. Nicosia, P. Tomei, "Design of Global Tracking Controllers for Flexible-Joint Robots," *Journal of Robotic Systems, vol. 109, pp. 310-319, 1993.*

[14] G. Tonietti, R. Schiavi, A. Bicchi, "Design and control of a variable stiffness actuator for safe and fast physical human/robot interaction," *IEEE International Conference on Robotics and Automation, pp. 526-531, 2005.*

[15] F. Petit, A. Dietrich, A. Albu-Schäffer, "Generalizing Torque Control Concepts: Using Well-Established Torque Control Methods on Variable Stiffness Robots," *IEEE Robotics and Automation Magazine, vol. 22, no. 4, pp. 37-51, 2015.*

[16] P. Tomei, "A Simple PD Controller for Robots with Elastic Joints," *IEEE Transactions on Automatic Control, vol. 36, pp. 1208-1213 1991.*

[17] A. de Luca, B. Siciliano, L. Zollo, "PD control with on-line gravity compensation for robots with elastic joints: Theory and experiments," *Automatica, vol. 41, no. 10, pp. 1809–1819, 2005.*

[18] M. Keppler, D. Lakatos, C. Ott, "Elastic Structure Preserving (ESP) Control of Compliantly Actuated Robots," *IEEE Transactions on Robotics, vol. 1, no. 2, pp. 1-19, 2018.*

[19] E. Spyrakos-Papastavridis, J. S. Dai, "Minimally Model-based Trajectory Tracking and Variable Impedance Control of Flexible-Joint Robots," *IEEE Transactions on Industrial Electronics, vol. 68, no. 7, pp. 6031-6041, 2021.*

[20] E. Spyrakos-Papastavridis, Z. Fu, J. S. Dai, "Power-Shaping Model-based Control with Feedback Deactivation for Flexible-Joint Robot Interaction," *IEEE Robotics and Automation Letters, vol. 7, no. 2, 2022.*

[21] A. Loria, R. Ortega, "On tracking control of rigid and flexible joint robots," *Appl. Math. Comput. Sci.*, vol. 5, no. 2, pp. 101–113, 1995.

[22] H. Dong et al., "Enabling Massage Actions: An Interactive Parallel Robot with Compliant Joints," *IEEE/RSJ International Conference on Intelligent Robots and Systems, 2022*

[23] C. Della Santina et al., "Model-based dynamic feedback control of a planar soft robot: trajectory tracking and interaction with the environment," *The International Journal of Robotics Research, vol. 39, no. 4, pp. 490-513, 2020.*

[24] G. Palli, C. Melchiorri, A. De Luca, "On the Feedback Linearization of Robots with Variable Joint Stiffness," *IEEE International Conference on Robotics and Automation, pp. 1753–1759, 2008.*

[25] E. Spyrakos-Papastavridis, P. Childs, J. S. Dai, "Passivity preservation for variable impedance control of compliant robots," *IEEE/ASME Transactions on Mechatronics*, *vol. 25, no. 5, pp. 2342-2353, 2020.*

[26] E. Spyrakos-Papastavridis, J. S. Dai, "Stable Flexible-Joint Floating-base Robot Balancing and Locomotion via Variable Impedance Control," *IEEE Transactions on Industrial Electronics, vol. 70, no. 3, pp. 2748-2758, 2022.*

[27] E. Spyrakos-Papastavridis, J. S. Dai, "Flexible-Joint Humanoid Balancing Augmentation via Full-State Feedback Variable Impedance Control," *ASME Journal of Mechanisms and Robotics, vol. 13, 021014, 2021.*

[28] E. Spyrakos-Papastavridis et al., "Online impedance regulation techniques for compliant humanoid balancing," *Robotics and Autonomous Systems, vol. 104, pp. 85-98, 2018.*

[29] E. Spyrakos-Papastavridis, P. Childs, N. G. Tsagarakis, "Variable Impedance Walking using Time-Varying Lyapunov Stability Margins," *IEEE-RAS International Conference on Humanoid Robots, pp. 318-323, 2017.*

[30] K. Kronander, A. Billard, "Stability Considerations of Variable Impedance Control," *IEEE Transactions on Robotics, vol. 32, no. 5, pp. 1298-1305, 2016.*

[31] F. Ferraguti et al., "An Energy Tank-Based Interactive Control Architecture for Autonomous and Teleoperated Robotic Surgery," *IEEE Transactions on Robotics, vol. 31, no. 5, pp. 1073-1088, 2015.*

[32] R. Wu, A. Billard, "Learning from Demonstration and Interactive Control of Variable-Impedance to Cut Soft Tissues," *IEEE/ASME Transactions on Mechatronics, DOI: 10.1109/TMECH.2021.3123356, 2021.*

[33] Y. Michel, C. Ott, D. Lee, "Safety-Aware Hierarchical Passivity-based Variable Impedance Control for Redundant Manipulators," *IEEE Transactions on Robotics, DOI: 10.1109/TRO.2022.3174478, 2022.*

[34] E. Spyrakos-Papastavridis, J. S. Dai, "A Model-Free Solution for Stable Balancing and Locomotion of Floating-base Legged Systems," *IEEE/RSJ International Conference on Intelligent Robots and Systems, pp. 3816-3822, 2020.*

[35] G. Buondonno, A. De Luca, "A recursive Newton-Euler algorithm for robots with elastic joints and its application to control," *IEEE/RSJ International Conference on Intelligent Robots and Systems, pp. 5526-5532, 2015.*

[36] M. Keppler, "Analyzing the Performance Limits of Articulated Soft Robots Based on the ESPi Framework: Applications to Damping and Impedance Control," *IEEE Robotics and Automation Letters, vol. 6, no .4, 2021.*

[37] M. Spong, "Modeling and control of elastic joint robots," *IEEE Journal on Robotics and Automation, vol. 3, pp. 291-300, 1987.*

[38] J. E. Slotine, W. Li, "On the adaptive control of robot manipulators," *The International Journal of Robotics Research, vol. 6, pp. 49-59, 1987.*

[39] I. Barkana, "Defending the Beauty of the Invariance Principle," *International Journal of Control, vol. 87, no. 1, pp. 186-206, 2014.*

[40] A. van der Schaft, L_2-Gain and Passivity Theorem Techniques in Nonlinear Control, *Springer-Verlag, no. 2, 2000.*

[41] [Online]. Available: https://sdk.rethinkrobotics.com/wiki/Hardware_Specifications#Joint_Flexure_Stiffness.

[42] E. Spyrakos-Papastavridis et al., "Online impedance parameter tuning for compliant biped balancing," *IEEE-RAS International Conference on Humanoid Robots, pp. 210-216, 2015*.

[43] E. Spyrakos-Papastavridis, D. Caldwell, N. G. Tsagarakis, "Balance and Impedance Optimization Control for Compliant Humanoid Stepping," *IEEE/RSJ International Conference on Intelligent Robots and Systems, pp. 1349-1355, 2016.*

[44] M. J. Pollayil et al., "Choosing Stiffness and Damping for Optimal Impedance Planning," *IEEE Transactions on Robotics, vol. 39, no. 2, 2023.*

Emmanouil Spyrakos-Papastavridis received the B.Sc. degree in electronic and electrical engineering from University College London (UCL), London, U.K., the M.Sc. degree in mechatronics from King's College London (KCL), London, U.K., and the Ph.D. degree in humanoid robotics from Istituto Italiano di Tecnologia (IIT), Genoa, Italy. He was a Postdoctoral Researcher with the Department of Advanced Robotics, Istituto Italiano di Tecnologia, a visiting researcher at the Dyson School of Design Engineering, Imperial College London, and a Postdoctoral Research Associate with the Department of Engineering, King's College London. He is currently a Lecturer (Assistant Professor) in robotics at the Centre for Robotics Research, Department of Engineering, King's College London. His research interests include flexible-joint systems, nonlinear control, optimal control, humanoids, bipedal balancing, legged systems, impedance control, and human-robot interaction. Dr. Spyrakos was a finalist for the Best Interactive Paper Award at Humanoids 2015, and is currently Principal Investigator of the Engineering and Physical Sciences Research Council (EPSRC) REST project.

Jian S. Dai (S'14–F'17) received the under-graduate and master's degrees in mechanical engineering from Shanghai Jiao Tong University, Shanghai, China, in 1982 and 1984, respectively, and the Ph.D. degree in advanced kinematics, mechanisms, and robotics from the University of Salford, Salford, U.K., in 1993. He is a Chair Professor of mechanisms and robotics with the Centre for Robotics Research, King's College London, University of London, London, U.K. He has been working in the field of mechanisms and robotics for the past 30 years and has authored or coauthored more than 600 peer-reviewed papers (more than 350 on ISI journals). His research interests include theoretical and computational kinematics, reconfigurable mechanisms, dexterous mechanisms and manipulators, end effectors, and multifingered hands. Dr. Dai is a Fellow of the Royal Academy of Engineering, the American Society of Mechanical Engineers (ASME), and the Institution of Mechanical Engineers. He was the recipient of the Mechanisms and Robotics Award, given annually by the Mechanisms and Robotics Committee of the ASME to engineers known for a lifelong contribution in the field of mechanism design or theory as the 27th recipient since 1974. He was also a recipient of the 2020 ASME Machine Design Award; the 58th recipient since the Award was established in 1958. He was a recipient of several journal and conference best paper awards. He is the Editor-in-Chief of Robotica, an Associate Editor for the ASME Transactions: *Journal of Mechanisms and Robotics*, and Subject Editor of *Mechanism and Machine Theory*.